COMMUNICATIONS IN SCIENCE AND TECHNOLOGY
Homepage: cst.kipmi.or.id

Investigation of hexanal removal through adsorption and photocatalysis on ZIF-7 modified with ZnO, TiO_2, and ZnO/TiO_2 using ATR-FTIR

Widyan Muhammad Naufal, Sayekti Wahyuningsih*, Witri Wahyu Lestari

Inorganic Material Research Group, Department of Chemistry, Universitas Sebelas Maret, Surakarta 57126, Indonesia

Article history:
Received: 16 August 2024 / Received in revised form: 15 October 2024 / Accepted: 15 October 2024

Abstract

Zeolitic imidazolate framework (ZIF) is renowned for its high adsorption capacity and frequently adsorbs organic pollutants. However, its high band gap energy has limited its photocatalytic activity, thus necessitating a modification for enhance performance enhancement. This study focuses on developing a ZIF-7 composite material that integrates adsorption and photocatalysis to remove volatile organic compounds (VOCs), particularly hexanal. Modifications were made by incorporating ZnO, TiO_2, and ZnO/TiO_2 via a solvothermal method using dimethylformamide (DMF). ATR-FTIR analysis was employed to monitor any changes in peak intensity related to the C=O vibrations of hexanal around 1700 cm^{-1}. The results showed that all samples effectively adsorbed hexanal, reducing peak intensity after UV irradiation, and confirming successful photocatalysis. Notably, TiO_2@ZIF-7 exhibited the highest photocatalytic performance with 88.06% degradation efficiency. This study confirms that the ATR-FTIR method can be used to monitor the success of adsorption and photocatalysis and shows the potential for developing composite materials to remove VOCs such as hexanal.

Keywords: ZIF-7; hexanal; adsorption; photocatalysis; ATR-FTIR

1. Introduction

Volatile organic compounds (VOCs) are easily vaporized organic chemicals that possess high mobility and resilience, allowing them to rapidly disperse in the environment upon release. VOC emissions are frequently detected in various products and ambient environments, with excessive emissions posing detrimental effects on both environment and human health [1,2]. Hexanal is one of the VOCs commonly encountered in daily life, such as in the organic synthesis, rubber, and paint industries [3]. However, it is also categorized as a major indoor irritant emanating from wooden furniture, furniture coating compounds, and panel boards. This compound is known for its strong, distinctive odor that can disrupt the human sense of smell [4]. In recent years, adsorption using various carbon materials has been the most commonly used removal method [5]. This method, however suffers from low adsorption capacity and can lead to adsorbent blockage. Furthermore, the trapped adsorbate within the adsorbent material requires further treatment [6]. Therefore, alternative processes are deemed necessary to address these issues, such as integrating environmentally friendly adsorption and photocatalysis processes that enhance degradation efficiency [7]. The development of materials capable of supporting these processes, as a result, is of significant importance.

One promising candidate material is metal-organic frameworks (MOF) considering their unique characteristics, such as high porosity, large specific surface area, and abundant active sites [8]. Additionally, the numerous weak interactions within MOF allow for the adjustment of building unit orientation, providing good structural stability. These interactions also enable MOF to effectively adsorb VOC molecules [9]. Of various types of MOF, zeolitic imidazolate framework (ZIF) is particularly attractive for their high adsorption capacity, chemical stability, and thermal stability [10]. ZIF-7 stands out as a superior adsorbent due to its π-π stacking interactions and gate-opening effects [11]. Several studies have explored the adsorption capabilities of ZIF-7. For instance, [12] reported that ZIF-7 had a CH_4 adsorption capacity of 0.065 mmol/g at 1 atm pressure and at 30 °C. Another study by [13] demonstrated that ZIF-7 could adsorb n-hexane, benzene, toluene, butyl acetate, p-xylene, styrene, mesitylene, and undecane with adsorption efficiencies ranging from 27.27% to 53.86%. However, the high bandgap energy of ZIF-7 still limits its photocatalytic activity [14], yet this issue can be addressed by modifying ZIFs with semiconductor materials to enhance their photocatalytic performance.

Metal oxide-based semiconductor materials such as SnO_2, SiO_2, Cu_2O, MgO, TiO_2, and ZnO have been widely used as

* Corresponding author.
Email: sayekti@mipa.uns.ac.id
https://doi.org/10.21924/cst.9.2.2024.1505

photocatalysts. Of these semiconductors, ZnO and TiO_2 are the most extensively studied due to their high photocatalytic activity, relatively low cost, good stability, and non-toxicity. Both materials also possess nearly identical band gaps [15,16, 17]. Scientists have extensively explored the combination of ZnO and TiO_2. As revealed by several studies, the ZnO/TiO_2 combination could exhibit enhanced stability and improve light scattering for visible light. Therefore, ZnO, TiO_2, and their combination ZnO/TiO_2 present promising potential for the degradation of organic contaminants such as VOCs [18,19].

In this work, the development of a material integrating adsorption and photocatalysis processes was achieved by modifying ZIF-7 with ZnO, TiO_2, and ZnO/TiO_2 semiconductors. The synthesis of the ZIF-7 composite was conducted through a solvothermal method with N,N-Dimethylformamide as the solvent. ZIF-7 serves as the adsorbent, while the addition of ZnO, TiO_2, and ZnO/TiO_2 aims to lower the band gap energy of ZIF-7, thereby enhancing its photocatalytic activity. The resulted ZIF-7 composites were then coated onto nonwoven fabric to facilitate their application in daily life. The adsorption and photocatalytic capabilities of these materials were tested on hexanal. Based on the literature review, the modification of ZIF-7 with ZnO, TiO_2, and ZnO/TiO_2 for applications in integrated adsorption and photocatalysis processes, so far, has not been previously explored. This research is expected to contribute to environmental treatment technology by offering more effective applications for pollutant management, particularly VOCs.

2. Materials and Methods

2.1. Materials

Zinc nitrate hexahydrate ($Zn(NO_3)_2.6H_2O$) was purchased from Himedia. Hexanal, imidazole (Im) (≥99%), benzimidazole (BIm) (≥98%), hexanal (≥97%), and titanium dioxide (TiO_2) (≥99%) were obtained from Sigma-Aldrich. Meanwhile, N,N-Dimethylformamide (DMF) was purchased from Loba Chemie and zinc oxide (ZnO) were obtained from Merck. Distilled water was supplied by CV. Agung Jaya Surakarta. All reagents used in this study were analytical grade ones and were used without further purification. Nonwoven fabric 20 cm in length and 7 cm in width, was supplied by Orenatural Surabaya.

2.2. Synthesis of ZnO/TiO_2

The synthesis of ZnO/TiO_2 was conducted by modifying the research [16,20]. Zinc oxide (0.163 g) and titanium dioxide (0.079 g) were mixed and ground in a mortar. The mixture was then placed in a furnace for 3 hours at a temperature of 500 °C.

2.3. Synthesis of ZIF-7

ZIF-7 was synthesized by modifying the research [21] through a solvothermal method. Each zinc nitrate hexahydrate (0.298 g), imidazole (0.136 g), and benzimidazole (0.119 g) was dissolved in 10 mL of DMF. The dissolution process involved stirring and sonication for 20 minutes. The benzimidazole and imidazole solutions were then mixed into the zinc nitrate solution. The mixture was stirred and transferred to an autoclave and heated in an oven at 120 °C for 48 hours. The resulted ZIF-7 particles, afterward, were washed with DMF three times and dried at 120 °C for 12 hours.

2.4. Synthesis of ZIF-7 composites

The synthesis procedure for the ZIF-7 composite was similar to that of ZIF-7 in which- each zinc nitrate hexahydrate (0.298 g), imidazole (0.136 g), and benzimidazole (0.119 g) was dissolved in 10 mL of DMF. The dissolution process involved stirring and sonication for 20 minutes. The benzimidazole and imidazole solutions were then mixed into the zinc nitrate solution. ZnO, TiO_2, or ZnO/TiO_2 (0.1 g) was added to the mixture for each synthesis. Subsequently, the mixture was stirred and heated in an autoclave at 120 °C for 48 hours. The resulted precipitate was washed with DMF three times and dried at 120 °C for 12 hours.

2.5. ZIF-7 composites coating on nonwoven fabric

Nonwoven fabric pieces with a diameter of 4 cm were prepared for the coating process. ZIF-7 composite (0.01 g) was dispersed in 2 mL of distilled water and sonicated for 10 minutes. The resulted suspension was then uniformly coated onto the nonwoven fabric using a dip-coating method. The samples were dried in an oven at 105 °C for 5 hours.

2.6. Adsorption and photocatalysis test on hexanal

The ZIF-7 composites coated on nonwoven fabric was placed above a hexanal solution using a tripod. The container was then heated at 140 °C to evaporate all the hexanal. The adsorption process was conducted for 4 hours. The adsorption capacity of the ZIF-7 composites was calculated using Equation 1, where Q refers to the adsorption capacity (mmol/g), Mr is the molecular mass of hexanal (g/mol), W_0 is the initial mass of the adsorbent (g), and W_1 is the mass of the adsorbent after hexanal adsorption (g).

$$Q = \frac{[1000 \times (W_1 - W_0)]}{[W_0 \times Mr]} \quad (1)$$

The degradation efficiency was tested immediately after the adsorption process was completed. The adsorbent material was irradiated with UV light for 2 hours. Later on, the adsorbent was analyzed by means of ATR-FTIR to observe any changes in peak intensity in the wavenumber region of 1700 cm^{-1}. The degradation percentage of the composite was calculated using Equation 2, where R is the hexanal degradation efficiency (%), I_0 is the initial peak intensity in the 1700 cm^{-1} region, and I_t is the peak intensity after 2 hours of irradiation in the 1700 cm^{-1} region.

$$R = \frac{[I_0 - I_t]}{I_0} \times 100\% \quad (2)$$

2.7. Characterizations

The evaluation of the crystal structure of the synthesized particles was performed by means of X-ray diffraction (XRD Bruker D8 Advance) with Cu Kα radiation in the 2θ range of

10–80°, operating at 40 kV and a current of 30 mA. Infrared spectra were tested using FTIR Shimadzu IR Prestige-21 in the wavenumber range of 4000-400 cm^{-1} with the KBr pellet method and ATR-FTIR Agilent Cary 60 in the wavenumber range of 4000-650 cm^{-1}. Meanwhile, particle morphology was obtained through a scanning electron microscope by JEOL JSM 6510. The optical characteristics of the ZIF-7 composite were analyzed using a UV-Vis spectrophotometer at a wavelength range of 200-800 nm with a scanning speed of 600 nm/min. The band gap of the ZIF-7 composite was determined through the Tauc plot method with the similar instrument. The specific surface area was measured in accordance to Brunauer-Emmett-Teller (BET) analysis based on N_2 adsorption-desorption via Nova® Surface Area Analyzer with a degassing temperature of 220 °C for 2 hours. Meanwhile, pore size distribution was determined using the Barrett-Joyner-Halenda (BJH) model with an equal instrument. The obtained data were further analyzed with the help of Origin 2022 software.

3. Results and Discussion

3.1. Characterization of ZnO/TiO₂

Fig. 1 presents the XRD patterns of ZnO, TiO_2, and the ZnO/TiO_2 composite. Here, the XRD pattern of ZnO exhibited the peaks at 2θ = 31.77º, 34.42º, 36.24º, 47.51º, 56.56º, 62.83º, 66.36º, 67.93º, 69.08º, 72.56º, and 76.93º, corresponding to the (100), (002), (101), (102), (110), (103), (200), (112), (201), (004), and (202) planes, respectively. This indicated the wurtzite phase [22]. This pattern aligns with the JCPDS standard 36-1451. In the meantime, the XRD pattern of TiO_2 displays peaks at 2θ = 25.25º, 36.92º, 37.74º, 38.61º, 47.99º, 53.85º, 54.95º, 62.66º, 68.59º, 70.23º, and 74.98º, corresponding to the (101), (103), (004), (112), (200), (105), (211), (204), (116), (220), and (215) planes, respectively, indicating the anatase phase [23]. This pattern is consistent with the JCPDS standard 21-1272. Furthermore, the XRD pattern of the ZnO/TiO_2 composite shows peaks from both precursors, confirming the successful synthesis.

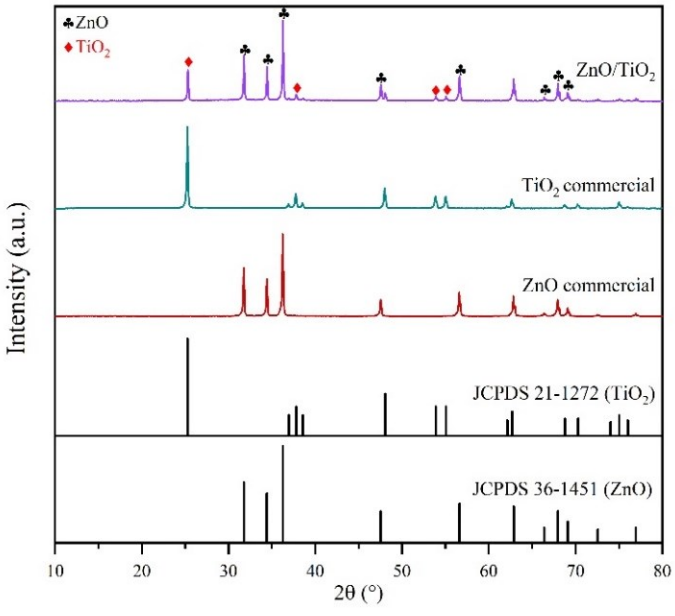

Fig. 1. XRD patterns of ZnO, TiO_2, and ZnO/TiO_2

3.2. Characterization of ZIF-7 composites

The crystal structure of ZIF-7 and the ZIF-7 composites, as shown in Fig. 2, was analyzed using XRD. The diffraction pattern exhibited the characteristic peaks of ZIF-7 at 2θ = 12.07º, 13.32º, 15.42º, 16.27º, 18.67º, and 19.62º, corresponding to the (012), (300), (220), (21$\bar{2}$), (401), and (13$\bar{2}$) planes. This pattern is consistent with [24]. When modified with the addition of TiO_2, the characteristic peaks of ZIF-7 showed minimal changes, though their intensity significantly decreased, indicating that adding TiO_2 does not drastically alter the crystal structure of ZIF-7. Conversely, the appearance of characteristic TiO_2 peaks confirms the success of the modification process. On the other hand, adding ZnO and ZnO/TiO_2 decreased intensity and irregularity in the characteristic peaks of ZIF-7, indicating that ZnO restricts the crystal growth of ZIF-7 [25]. Nonetheless, the presence of characteristic peaks of ZnO and ZnO/TiO_2 indicates the success of the modification process.

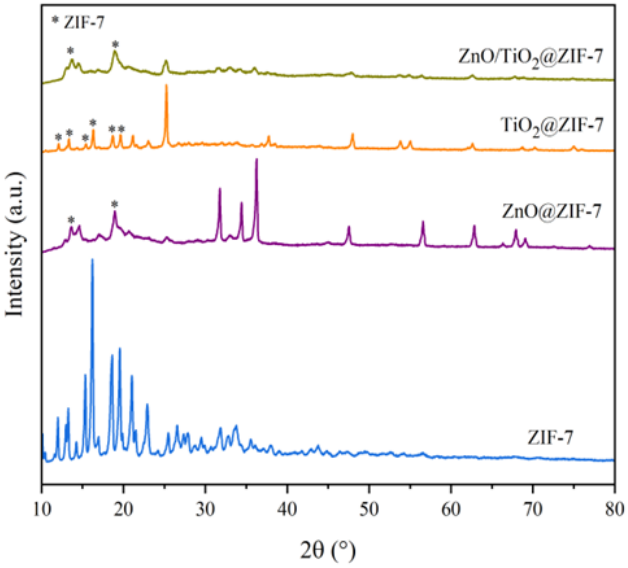

Fig. 2. XRD pattern of ZIF-7 and ZIF-7 composites

Fig. 3 illustrates the SEM images of ZIF-7 and ZIF-7 composites. Fig. 3(a) shows that ZIF-7 exhibited a uniform cubic shape with an average particle size of approximately 1.53 µm, consistent with [26]. When TiO_2 was added, the particle morphology was observed as well (Fig. 3(b)), where TiO_2 granules appeared near ZIF-7 particles. However, with the addition of ZnO and ZnO/TiO_2 (Fig. 3(c) and 3(d)), only a small portion of the ZIF-7 particles could be observed. Nonetheless, the visible ZIF-7 particles did not entirely maintain a perfect cubic shape.

Based on data regarding XRD and SEM, modifications with ZnO and ZnO/TiO_2 are capable of altering the crystal structure of ZIF-7 [27]. This phenomenon is believed to occur due to the competition between zinc nitrate precursor and ZnO during the crystal formation. Research [28] indicated that ZnO particles facilitated the nucleation process, which could accelerate the formation of MOFs. Therefore, ZnO acts as an effective precursor for the nucleation of various MOFs, particularly those based on Zn. However, other precursors, such as zinc

nitrate, can interfere by forming these frameworks. This leads to competition among linkers to form the MOF network with zinc nitrate and ZnO, ultimately causing irregularities in particle shape.

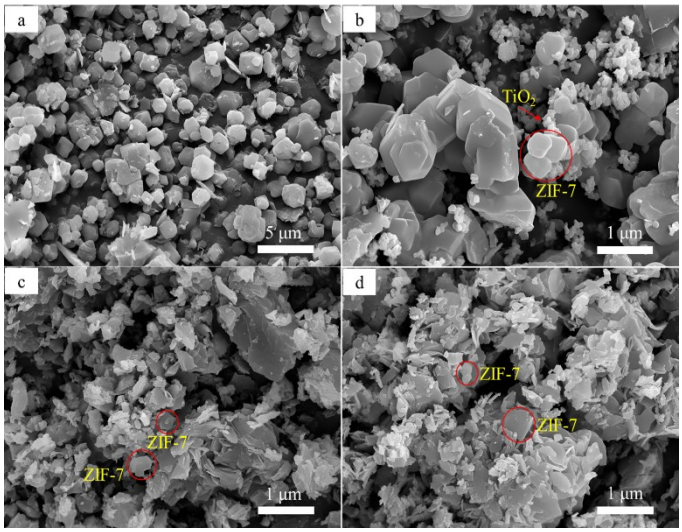

Fig. 3. SEM image of (a) ZIF-7, (b) TiO_2@ZIF-7, (c) ZnO@ZIF-7, (d) ZnO/TiO_2@ZIF-7

FTIR was utilized to identify the functional groups within the synthesized material, as displayed in Fig. 4. Absorption peaks at wavenumbers 1605 cm^{-1}, and 1243 cm^{-1} indicated C=N stretching and C-N stretching vibrations from benzimidazole. The vibrations of C=C and out-of-plane C-H from the benzene ring in benzimidazole were observed at peaks 1474 cm^{-1} and 742 cm^{-1}. Absorptions at 1089 cm^{-1} and 952 cm^{-1} are attributed to in-plane C-H bending in benzimidazole [29]. A peak around 516 cm^{-1} indicates Zn-N stretching vibrations originating from the bond between the linker and the central atom [30]. These absorptions confirm the successful formation of ZIF-7. However, the synthesis was partially pure, as some impurities were detected. Peaks at 3660 cm^{-1} and 3431 cm^{-1} are identified as stretching vibrations of adsorbed water and hydrogen bonding of water molecules adsorbed on ZIF-7 [31]. Furthermore, absorption at 1676 cm^{-1} indicates carbonyl stretching vibrations from DMF [32], which is further supported by peaks at 3051 cm^{-1} and 2928 cm^{-1} corresponding to C-H stretching vibrations from DMF [33].

The modification process did not significantly affect the functional groups of ZIF, except with the addition of TiO_2. A broadened peak with strong intensity at 742 cm^{-1} was observed, attributed to the O-Ti-O vibration [34]. The broadening of this peak is likely due to the superimposition of Ti-O stretching bands from TiO_2 [16]. However, modifications with ZnO/TiO_2 did not show any TiO_2 vibrations, which may be due to the low composition of this compound. In addition, the interaction of TiO_2 with ZnO or the overlapping of the absorption bands of the two compounds can also cause the specific TiO_2 peak to become undetectable or not visible.

Fig. 5 illustrates the optical characteristics of the synthesized compounds. ZIF-7 exhibited two types of peaks at wavelengths of 274 nm and 280 nm, corresponding to the $\pi \rightarrow \pi^*$ transition of the azomethine group and the $n \rightarrow \pi^*$ transition due to the charge transfer between C=N in benzimidazole [35]. Tauc plot analysis revealed that the band gap energy of ZIF-7 was 5.66 eV (Fig. 5(a)). After modification, each ZIF-7 composite exhibited a blue shift and the emergence of a new peak at 243 nm. The incorporation of semiconductor materials reduced the band gap energy of ZIF-7 due to the interaction of valence electrons from the semiconductor material with the electronic structure of ZIF-7, resulting in changes in the orbital energy distribution. The decrease in the band gap from 5.66 eV to 4.25-4.61 eV indicated that the energy levels of the metal oxide have blended with the energy levels in ZIF-7, indicating that the metal oxide has successfully integrated electronically with ZIF-7 (Fig. 5(b)). As a result, the ZIF-7 composite is more likely to undergo optical transitions at lower energies, thus producing more electron-hole pairs, which later on impact on the increasing photocatalytic efficiency [36].

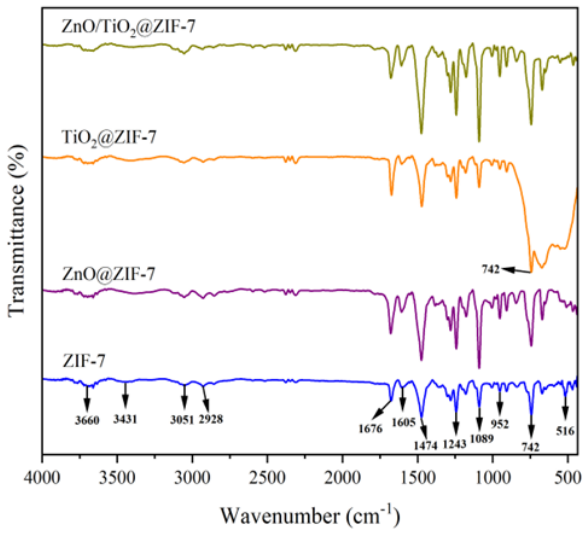

Fig. 4. FTIR spectrum of ZIF-7 and ZIF-7 composites

The modified materials' BET surface area and pore distribution showed significant changes compared with pure ZIF-7 (Table 1), which directly affected the materials' adsorption capacity and photocatalytic performance. Here, ZIF-7 showed the highest BET surface area with a pore radius of 4.77 nm. This result differs from the theoretical calculation, showing that solvent-free ZIF-7 should have a surface area of about 405 m^2/g. This difference is due to the residual DMF solvent in ZIF-7, which clogs the total porosity and reduces the accessibility of nitrogen to the internal cavities of ZIF-7 [37]. The decrease in surface area was observed after modification with ZnO, TiO_2, and ZnO/TiO_2, indicating that metal oxide particles were deposited on the surface and inside the pores of ZIF-7, thereby reducing the surface area available for interaction with target molecules. Modification with ZnO and ZnO/TiO_2 increased pore size due to the disruption or collapse of the ZIF-7 framework. This collapse is due to the interaction between ZnO nanoparticles and the ZIF-7 framework, which results in pore enlargement or the merging of tiny pores into larger ones [38]. In contrast, modification with TiO_2 decreases pore size, indicating that TiO_2 tends to be distributed more evenly across the ZIF-7 surface, with a tendency to enter tiny pores and partially close the porosity [39].

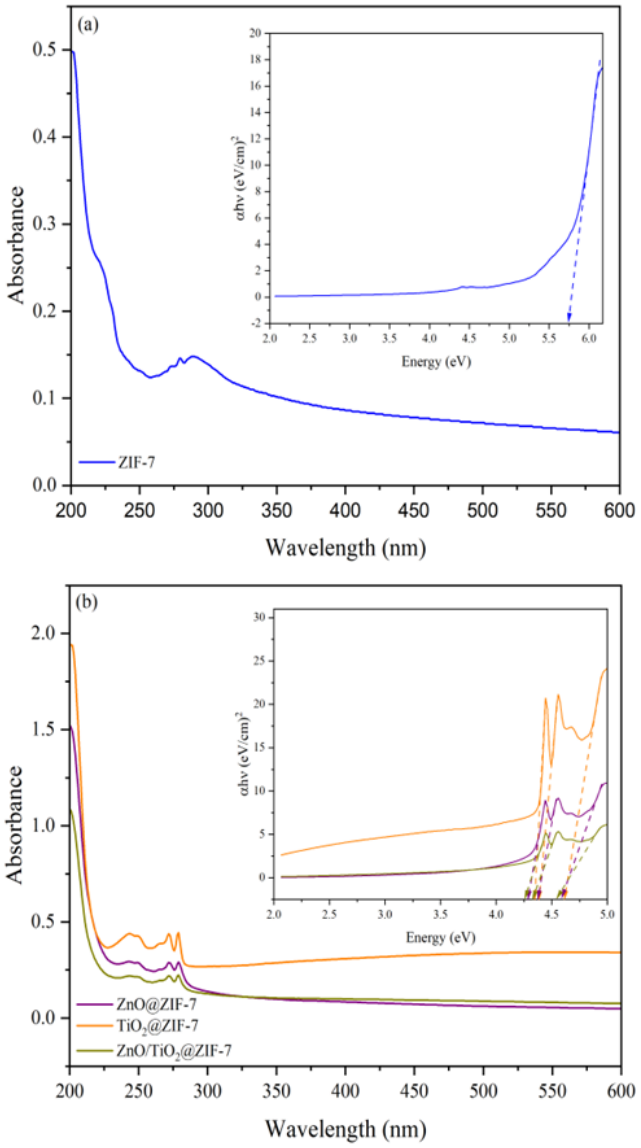

Fig. 5. UV-visible spectra and Tauc plots of (a) ZIF-7 and (b) ZIF-7 composites

Table 1. Summary of BET measurements

Sample	Surface Area (m^2 g^{-1})	Pore Volume (cm^3 g^{-1})	Average Pore Diameter (nm)
ZIF-7	128.4	0.037	4.77
ZnO@ZIF-7	7.127	0.008	4.81
TiO_2@ZIF-7	30.68	0.03	4.74
ZnO/TiO_2@ZIF-7	18.54	0.083	4.80

3.3. Adsorption and photocatalysis test on hexanal

As visualized in Fig. 6, peaks at 2951 cm^{-1} and 2917 cm^{-1} corresponded to the asymmetric stretching vibrations of CH_3 and CH_2. The symmetric stretching vibrations of CH_2 were also observed at 2869 cm^{-1}. Additionally, peaks at 1457 cm^{-1} and 1375 cm^{-1} were identified as the symmetric bending of CH_2 and CH_3. All identified peaks indicate that the nonwoven fabric is composed of polypropylene [40]. After coating, changes in the peaks within the 1250-650 cm^{-1} range were observed, consistent with the FTIR spectrum as shown in Fig. 4. This confirms the successful coating process on the nonwoven fabric.

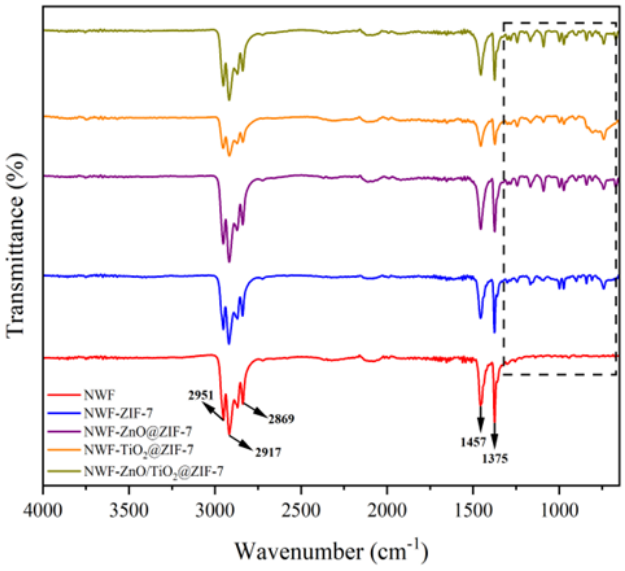

Fig. 6. ATR-FTIR spectra of sample before and after coating on nonwoven fabric

ATR-FTIR analysis is a method used to activate the adsorption and photocatalysis processes. ATR-FTIR provides qualitative information about the presence of certain compounds and can also be used to display quantitative changes in the peak intensity of information related to the concentration of target molecules. As a secondary method, ATR-FTIR analysis can still be used for quantitative calculations as it allows real-time so that the adsorption and photocatalysis processes can be detected quickly. In addition, hexanal, the target molecule, has a typical C=O absorption band in the range of 1700 cm^{-1}, allowing the quantification process. Based on the test results, Fig. 7a shows that each sample could adsorb hexanal, as indicated by the appearance of a peak around 1700 cm^{-1} as, the characteristic of C=O vibrations in hexanal. This peak's presence provided evidence of an interaction between the hexanal molecule and the active site on the sample surface. The peak is also used as a quantitative indicator to measure the adsorption capacity between samples. After UV irradiation, a decrease in peak intensity in the region was observed as shown Fig. 7b. The decrease in peak intensity can indicate that a photocatalysis process has occurred so that the hexanal molecule decomposes into more straightforward products that no longer provide strong signals at that wave number. The data also showed that each sample showed different adsorption and photocatalysis capabilities, as reflected by changes in peak intensity in the 1700 cm^{-1} region.

Fig. 8 presents the data on adsorption capacity and degradation efficiency and Fig. 8(a) illustrates the adsorption capacities of NWF-ZIF, NWF-ZnO@ZIF, NWF-TiO_2@ZIF, and NWF-ZnO/TiO_2@ZIF, with the values of 30.29 mmol/g, 11.57 mmol/g, 24.42 mmol/g, and 13.78 mmol/g, respectively. As confirmed by SEM data, the reduction in adsorption capacity observed with semiconductor modification was

attributed to the damage to the ZIF structure during modification. This finding aligns with previous literature reports indicating that adding metal oxide to MOF significantly reduces specific surface area [41,42,43]. Nevertheless, the enhanced photocatalytic activity resulting from these modifications may compensate for the decrease in adsorption capacity by improving pollutant degradation efficiency, as shown in Fig. 8(b). The degradation efficiencies of NWF-ZIF, NWF-ZnO@ZIF, NWF-TiO_2@ZIF, and NWF-ZnO/TiO_2@ZIF were 38.71%, 72.32%, 88.06%, and 81.91%, respectively. Overall, the degradation efficiency of the ZIF composites was found higher than that of NWF-ZIF due to the incorporation of semiconductors, reducing the band gap energy of the ZIF and facilitating the photocatalytic process [44]. The improvement in degradation efficiency emerges as a more critical factor in pollutant removal applications rather than adsorption capacity.

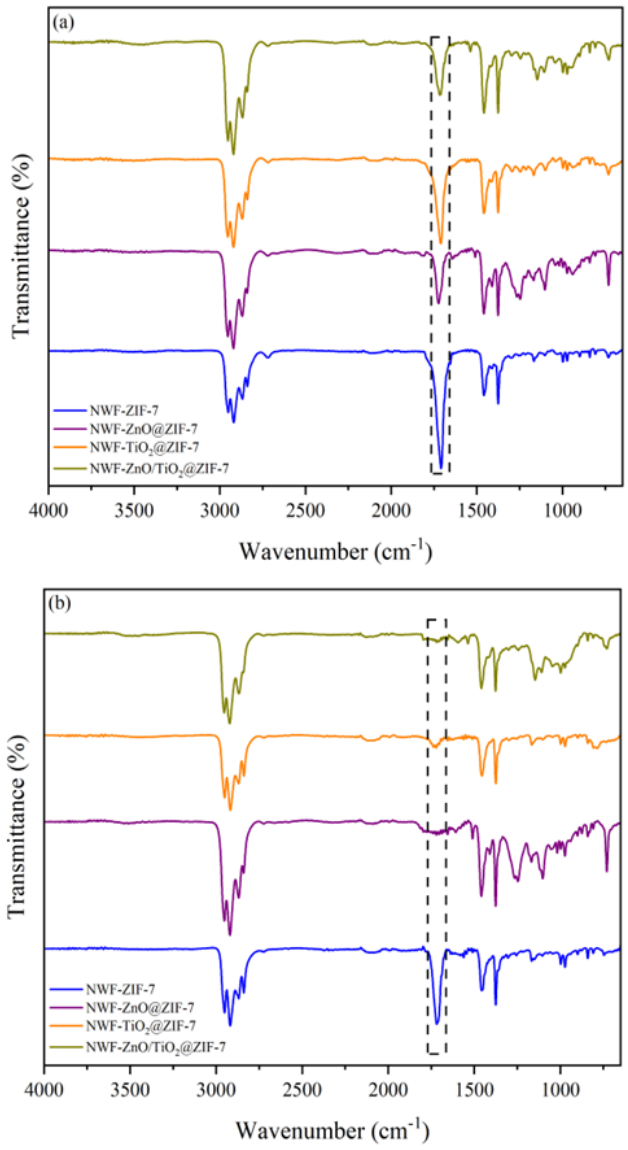

Fig. 7. ATR-FTIR spectra of sample (a) after the adsorption process for 4 hours and (b) after the irradiation process for 2 hours

The adsorption mechanism of ZIF composite for the hexanal test compound mainly occurred through the filling of mesopore cavities. This process unfolded as the adsorbate molecules swiftly disperse on the outer surface of the ZIF composite, inducing electrostatic interactions on the composite surface. Gradually, the adsorbate molecules migrated to the mesopore channels and were subsequently absorbed and stored within. Other adsorption mechanisms, such as hydrogen bonding or π–π interactions between the ZIF composite and hexanal, may also take place, enhancing the composite adsorption effect [6].

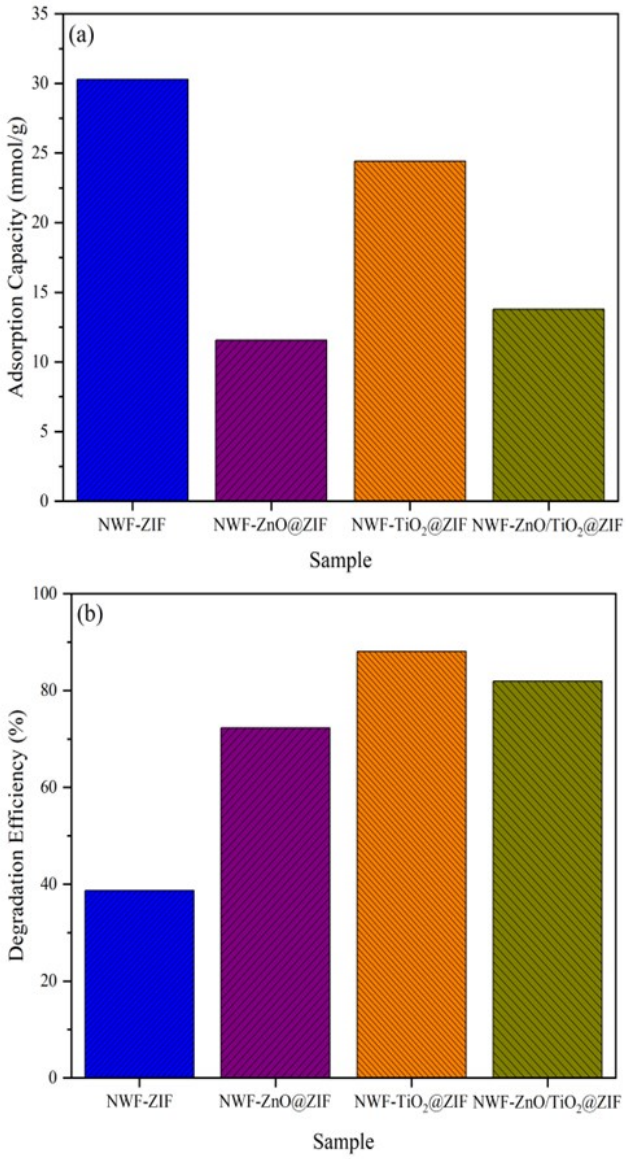

Fig. 8. Profile of (a) adsorption capacity and (b) degradation efficiency of sample on hexanal

Additionally, the photocatalytic degradation mechanism of hexanal can be elucidated as follows. Once hexanal is adsorbed onto the ZIF composite, it is exposed to UV light for 2 hours. This UV light facilitates the excitation of electrons from the valence band to the conduction band of the ZIF composite, generating electron-hole pairs (e^- and h^+). Electrons react with O_2 to form superoxide radicals, while holes react with H_2O to form hydroxyl radicals [45]. The presence of these free radicals enables the oxidation of hexanal into CO_2 and H_2O through various intermediate compounds such as C_4H_8CHO, C_4H_8, and so fort [46]. The reactions conform to equations 3-11.

$$\text{ZIF-7 composites} + hv \rightarrow e_{cb}^- + h_{vb}^+ \quad (3)$$

$$e_{cb}^- + O_2 \rightarrow \bullet O_2^- \quad (4)$$

$$\bullet O_2^- + H^+ \rightarrow HO_2\bullet \quad (5)$$

$$2HO_2\bullet \rightarrow O_2 + H_2O_2 \quad (6)$$

$$e_{cb}^- + H_2O_2 \rightarrow OH^- + \bullet OH \quad (7)$$

$$h_{vb}^+ + OH^- \rightarrow \bullet OH \quad (8)$$

$$h_{vb}^+ + H_2O \rightarrow H^+ + \bullet OH \quad (9)$$

$$C_5H_{11}CHO + \bullet OH \rightarrow CO_2 + H_2O \quad (10)$$

$$C_5H_{11}CHO + \bullet O \rightarrow CO_2 + H_2O \quad (11)$$

4. Conclusion

The modification of ZIF-7 with the addition of TiO_2, ZnO, and a combination of ZnO/TiO_2 significantly impacted its physicochemical properties and photocatalytic performance. The addition of TiO_2 did not drastically alter the crystal structure of ZIF-7, as indicated by the decreased intensity of characteristic peaks in the XRD pattern of ZIF-7. Meanwhile, adding ZnO and ZnO/TiO_2 led to a decrease in peak intensities and irregularities in the characteristic peaks of ZIF-7, providing deeper insights into the mechanism of ZIF modification using semiconductors. The semiconductor modification also decreased the adsorption capacity of ZIF-7, attributed to changes in the material's structure and surface properties. However, adding semiconductors could also lower the bandgap energy of ZIF-7, thereby enhancing the degradation efficiency towards hexanal, especially in the case of TiO_2, showing the efficiency value of 88.06%. Therefore, further research on the semiconductor addition ratio to ZIF-7 presents an interesting direction to optimize the adsorption and photocatalytic performance of the material without sacrificing a significant portion of its adsorption capacity.

Acknowledgements

The author would like to thank LPPM Sebelas Maret University for funding this fundamental research through the Research Contract Letter No 228/UN27.22/PT.01.03/2023. The author also thanks to Sebelas Maret Unversity Integrated Laboratory Services Unit, who provided technical assistance during this research.

References

1. Y. Xie, S. Lyu, Y. Zhang, and C. Cai, *Adsorption and degradation of volatile organic compounds by Metal–Organic Frameworks (MOFs): A Review*, Materials. 15 (2022) 7727.
2. R. Yadav, and P. Pandey, *A Review on Volatile Organic Compounds (VOCs) as environmental pollutants: Fate and distribution*, Int. J. Plant Environ. 4 (2018) 14–26.
3. D. Dhakshinamoorthy, S. Sundaresan, A. Iyadurai, K. S. Subramanian, G. J. Janavi, G. Paliyath *et al*., *Hexanal vapor induced resistance against major postharvest pathogens of banana (Musa acuminata L.)*, Plant Pathol. J. 36 (2020) 133–147.
4. Y. Cho, M. K. Song, T. S. Kim, and J. C. Ryu, *Identification of novel cytokine biomarkers of hexanal exposure associated with pulmonary toxicity*, Environ. Pollut. 229 (2017) 810–817.
5. E. David, and V. C. Niculescu, *Volatile organic compounds (VOCs) as environmental pollutants: Occurrence and mitigation using nanomaterials*, Int. J. Environ. Res. Public Health. 18 (2021) 13147.
6. H. Li, Y. Cheng, J. Li, T. Li, J. Zhu, W. Deng *et al*., *Preparation and adsorption performance study of graphene quantum dots@ZIF-8 composites for highly efficient removal of volatile organic compounds*, Nanomaterials. 12 (2022) 4008.
7. W. Zou, B. Gao, Y. S. Ok, and L. Dong, *Integrated adsorption and photocatalytic degradation of Volatile Organic Compounds (VOCs) using carbon-based nanocomposites: A critical review*, Chemosphere. 218 (2019) 845–859.
8. T. Wang, Y. Wang, M. Sun, A. Hanif, H. Wu, Q. Gu *et al*., *Thermally treated zeolitic imidazolate framework-8 (ZIF-8) for visible light photocatalytic degradation of gaseous formaldehyde*, Chem. Sci. 11 (2020) 6670–6681.
9. H. W. Wu, L. W. Lee, P. Thanasekaran, C. H. Su, Y. H. Liu, T. M. Chin *et al*., *Weak interactions in imidazole-containing zinc(II)-based metal–organic frameworks*, J. Chin. Chem. Soc. 67 (2020) 2182–2188.
10. L. Bogdan, A. Palčić, M. Duplančić, M. Leskovac, and V. Tomašić, *Eco-friendly synthesis of TiO_2/ZIF-8 composites: Characterization and application for the removal of imidacloprid from wastewater*, Processes. 11 (2023) 963.
11. N. Amareh, Y. Yamini, M. Saeidi, Z. Dinmohammadpour, and M. Nazraz, *Synthesis, characterization and application of ZIF-7@ZIF-67/PES for dispersive solid phase extraction of bisphenol A and 2-phenyl phenol*, Talanta Open. 8 (2023) 100269.
12. A. Arami-Niya, G. Birkett, Z. Zhu, and T. E. Rufford, *Gate opening effect of zeolitic imidazolate framework ZIF-7 for adsorption of CH_4 and CO_2 from N_2*, J. Mater. Chem. A. 5 (2017) 21389–21399.
13. Y. T. Zhao, L. Q. Yu, X. Xia, X. Y. Yang, W. Hu, and Y. K. Lv, *Evaluation of the adsorption and desorption properties of Zeolitic Imidazolate Framework-7 for volatile organic compounds through thermal desorption-gas chromatography*, Anal. Methods. 10 (2018) 4894-4901.
14. A. Semwal, D. Sajwa, J. Rawat, L. Gambhir, H. Sharma, and C. Dwivedi, *Carbon-doped TiO_2/ZIF-8 Composite for solar light harvested degradation of Methylene Blue*, Res Square. 21 (2022) 1-16.
15. M. A. Habib, M. T. Shahadat, N. M. Bahadur, I. M. I. Ismail, and A. J. Mahmood, *Synthesis and characterization of ZnO-TiO_2 nanocomposites and their application as photocatalysts*, Int. Nano Lett. 3 (2013) 5.
16. F. Hossain, M. A. Rahman, and M. M. Hossain, *ZnO-TiO_2 Composite mediated photocatalytic degradation of Orange G from aqueous solution*, Dhaka Univ. J. Sci. 69 (2022) 218–224.
17. A. S. Rini, Y. Rati, G. Maheta, A. P. Aji, and Saktioto, *Utilizing Pometia pinnata leaf extract in microwave synthesis of ZnO nanoparticles: Investigation into photocatalytic properties*, Commun. Sci. Technol. 9 (2024) 94-99.
18. M. M. Ali, M. J. Haque, M. H. Kabir, M. A. Kaiyum, and M. S. Rahman, *Nano synthesis of ZnO-TiO_2 composites by sol-gel method and evaluation of their antibacterial, optical and photocatalytic activities*, Results Mater. 11 (2021) 100199.
19. D. Ramírez-Ortega, A. M. Meléndez, P. Acevedo-Peña, I. González, R. Arroyo, *Semiconducting properties of ZnO/TiO_2 composites by electrochemical measurements and their relationship with photocatalytic activity*, Electrochim. Acta. 140 (2014) 541–549.
20. Y. Wang, X. Liu, L. Guo, L. Shang, S. Ge, G. Song *et al*., *Metal organic framework-derived C-doped ZnO/TiO_2 nanocomposite catalysts for enhanced photodegradation of Rhodamine B*, J. Colloid Interface Sci. 599 (2021) 566–576.

21. J. Yang, Y. B. Zhang, Q. Liu, C. A. Trickett, E. Gutiérrez-Puebla, M. Á. Monge *et al*., *Principles of designing extra-large pore openings and cages in Zeolitic Imidazolate Frameworks*, J. Am. Chem. Soc. 139 (2017) 6448–6455.
22. M. R. Arefi, and S. Rezaei-Zarchi, *Synthesis of zinc oxide nanoparticles and their effect on the compressive strength and setting time of self-compacted concrete paste as cementitious composites*, Int. J. Mol. Sci. 13 (2012) 4340–4350.
23. K. A. Kumar, K. Subalakshmi, and J. Senthilselvan, *Effect of mixed valence state of titanium on reduced recombination for natural dye-sensitized solar cell applications*, J. Solid State Electrochem. 20 (2016) 1921–1932.
24. Deposition numbers 602541 (for ZIF-7) contain the supplementary crystallographic data for this paper. These data are provided free of charge by the joint Cambridge Crystallographic Data Centre and Fachinformationszentrum Karlsruhe Access Structures service.
25. W. Yu, C. H. Lan, S. J. Wang, P. F. Fang, and Y. M. Sun, *Influence of zinc oxide nanoparticles on the crystallization behavior of electrospun poly(3-hydroxybutyrate-co-3-hydroxyvalerate) nanofibers*, Polymer. 51 (2010) 2403–2409.
26. H. Hu, S. Liu, C. Chen, J. Wang, Y. Zou, L. Lin et al., *Two novel zeolitic imidazolate frameworks (ZIFs) as sorbents for solid-phase extraction (SPE) of polycyclic aromatic hydrocarbons (PAHs) in environmental water samples*, Analyst. 139 (2014) 5818–5826.
27. D. Zhao, X. Wan, H. Song, L. Hao, Y. Su, and Y. Lv, *Metal-Organic Frameworks (MOFs) combined with ZnO quantum dots as a fluorescent sensing platform for phosphate*, Sens. Actuators, B. 197 (2014) 50–57.
28. E. Zanchetta, L. Malfatti, R. Ricco, M. J. Styles, F. Lisi, C. J. Coghlan et al., *ZnO as an efficient nucleating agent for rapid, room temperature synthesis and patterning of Zn-based Metal-Organic Frameworks*, Chem. Mater. 27 (2015) 690–699.
29. V. A. Polyakov, V. V. Butova, E. A. Erofeeva, A. A. Tereshchenko, and A. V. Soldatov, *MW synthesis of ZIF-7: The effect of solvent on particle size and hydrogen sorption properties*, Energies. 13 (2020) 6306.
30. E. G. Masibi, T. A. Makhetha, and R. M. Moutloali, *Effect of the incorporation of ZIF-8@GO into the thin-film membrane on salt rejection and BSA fouling*, Membranes. 12 (2022) 436.
31. K. Tan, S. Zuluaga, Q. Gong, P. Canepa, H. Wang, J. Li et al., *Water reaction mechanism in metal organic frameworks with coordinatively unsaturated metal ions: MOF-74*, Chem. Mater. 26 (2014) 6886–6895.
32. L. Frentzel-Beyme, P. Kolodzeiski, J. B. Weiß, A. Schneemann, and S. Henke, *Quantification of gas-accessible microporosity in metal-organic framework glasses*, Nat. Commun. 13 (2022) 7750.
33. P. Zhu, Y. Ma, Y. Wang, Y. Yang, and G. Qian, *Separation and recovery of materials from the waste Light Emitting Diode (LED) modules by solvent method*, J. Mater. Cycles Waste Manage. 22 (2020) 1184–1195.
34. E. Rusman, H. Heryanto, A. N. Fahri, I. Mutmainna, and D. Tahir, *Green synthesis ZnO/TiO_2 for high recyclability rapid sunlight photodegradation textile dyes applications*, MRS Adv. 7 (2021) 444–449.
35. T. Y. Fonkui, M. I. Ikhile, P. B. Njobeh, and D. T. Ndinteh, *Benzimidazole schiff base derivatives: Synthesis, characterization and antimicrobial activity*, BMC Chem. 13 (2019) 127.
36. N. T. T. Tu, L. H. Khang, N. N. P. Thao, N. T. T. Hien, T, T. Chau, L. T. H. Diep *et al*., *Zinc/Cobalt-based zeolite imidazolate frameworks for simultaneously degrading dye and inhibiting bacteria*, J. Nanomater. 2022 (2022) 8630685.
37. C. Cuadrado-Collados, J. Fernández-Català, F. Fauth, Y. Q. Cheng, L. L. Daemen, A. J. Ramirez-Cuesta *et al*., *Understanding the breathing phenomena in nano-ZIF-7 upon gas adsorption*, J. Mater. Chem. A. 5 (2017) 20938–20946.
38. S. Zhong, Q. Wang, and D. Cao, *ZIF-Derived nitrogen-doped porous carbons for Xe adsorption and separation*, Sci. Rep. 6 (2016) 21295.
39. H. Zheng, B. Zhong, Q. Wang, X. Li, J. Chen, L. Liu *et al*., *ZnO-Doped Metal-Organic Frameworks nanoparticles: Antibacterial activity and Mechanism*, Int. J. Mol. Sci. 24 (2023) 12238.
40. A. Gopanna, R. N. Mandapati, S. P. Thomas, K. Rajan, and M. Chavali, *Fourier transform infrared spectroscopy (FTIR), Raman spectroscopy and wide-angle X-ray scattering (WAXS) of polypropylene (PP)/cyclic olefin copolymer (COC) blends for qualitative and quantitative analysis*, Polym. Bull. 76 (2019) 4259–4274.
41. M. Jin, X. Qian, J. Gao, J. Chen, D. K. Hensley, H. C. Ho, R. J. Percoco, C. M. Ritzi, and Y. Yue, *Solvent-free synthesis of CuO/HKUST-1 composite and its photocatalytic applications*, Inorg. Chem. 58 (2019) 8332-8338.
42. Q. Li, Y. Wu, X. Ye, Y. Zeng, and M. Ding, *ZnO-based heterostructure constructed using HKUST-1 for enhanced visible-light photocatalytic hydrogen evolution*, Appl. Catal., A. 633 (2022) 118533.
43. M. Xiaobo, L. Xinyu, Z. Jie, H. Xiaoxian, and Y. Weichun, *Heterostructured TiO_2@HKUST-1 for the enhanced removal of methylene blue by integrated adsorption and photocatalytic degradation*, Environ. Technol. 42 (2021) 4134-4144.
44. S. Roy, J. Darabdhara, and M. Ahmaruzzaman, *ZnO-based Cu Metal-organic framework (MOF) nanocomposite for boosting and tuning the photocatalytic degradation performance*, Environ. Sci. Pollut Res, 30 (2023) 95673-95691.
45. C. Purnawan, S. Wahyuningsih, O. N. Aniza, and O. P. Sari, *Photocatalytic degradation of Remazol Brilliant Blue R and Remazol Yellow FG using TiO_2 doped Cd, Co, Mn*, Bull. Chem. React. Eng. Catal. 16 (2021) 804–815.
46. L. Miao, X. Tang, S. Zhao, X. Xie, C. Du, T. Tang *et al*., *Study on mechanism of low-temperature oxidation of n-hexanal catalysed by 2D ultrathin Co_3O_4 nanosheets*, Nano Res. 15 (2022) 1660–1671.